Acta Montanistica Slovaca
ISSN 1335-1788
actamont.tuke.sk

Spatio-Temporal Analysis of Yield Estimation of Corn and Sunflower Using Single-Dated Satellite Imagery Between 2014-2016

Pinar KARAKUS*[1], *Hakan KARABORK*[2]** *and* ***Sinasi KAYA*[3]**

Authors' affiliations and addresses:
[1] Geomatics Engineering, Osmaniye Korkut Ata University, Osmaniye, Türkiye
e-mail: pinarkarakus@osmaniye.edu.tr

[2] Geomatics Engineering, Konya Technical University, Konya, Türkiye
e-mail: hkarabork@ktun.edu.tr

[3] Geomatics Engineering, Istanbul Technical University, İstanbul, Türkiye
e-mail: kayasina@itu.edu.tr

***Correspondence:**
Pinar Karakus, Geomatics Engineering, Osmaniye Korkut Ata University, Osmaniye, Türkiye
tel.: 05063513596
e-mail: pinarkarakus@osmaniye.edu.tr

Funding information:
Selcuk University Scientific Research Project Grant Number 13101032

Acknowledgement:
This article is derived from Pınar KARAKUŞ's doctoral dissertation titled 'Identification of Agricultural Products and Yield Estimation with Multi-Temporal Satellite Image Data' (Ph.D. Dissertation, Selcuk University, Konya, Türkiye, 2017).

How to cite this article:
Karakus, P., Karabork, H. and Kaya, S. (2024). Spatio-Temporal Analysis of Yield Estimation of Corn and Sunflower Using Single-Dated Satellite Imagery Between 2014-2016**,** *Acta Montanistica Slovaca*, Volume 29 (4), 819-838

DOI:
https://doi.org/10.46544/AMS.v29i4.04

Abstract
Multi-temporal satellite images are generally used to calculate yield estimation. However, investigating the feasibility of yield estimation using a single-dated satellite image still needs to be solved today. The benefits of using a single-dated satellite image in yield estimation and optimum timing are among the issues to be considered in future studies.
This study developed a parcel-based yield model using a single satellite image for the 2014, 2015, and 2016 years and meteorological data in Kadirli-Osmaniye, Türkiye. The SPOT 6&7 satellite images were acquired at an appropriate time of the plant cover (the greenest period of the plant). For four months, photographs and values of plant height are provided weekly from fieldwork to determine crop cover fraction and monitor vegetation development. Regression analysis was performed with 12 vegetation indexes obtained from satellite images and crop cover fractions. In all calculated yield models, the relationship between I.-II.-III. soil classes selected, considering soil maps and yield, are compared. The relative errors of the low-yield fields were calculated between 10% and 35% (according to the yields obtained at harvest time). As a result, it was determined that a single satellite image could model yield estimation of corn and sunflower for each year on fields with an average of 0.10 relative errors.

Keywords
Sunflower; Corn; Single Date Satellite Image; Yield Estimation; Crop Cover Fraction (CCF)

Introduction

The increase in demand for agricultural products and the dependence of agricultural production on environmental conditions reveal the necessity of monitoring plant production. Monitoring and forecasting plant production, both on a regional and global scale, is significant for agricultural land management, food safety warning systems, food trade policies, and carbon cycle research (Tao et al., 2005; Karthikeyan et al., 2020).

Corn, consumed by about half of the world's population, is one of the most preferred grain products as animal feed worldwide. Among the oilseed plants cultivated in Türkiye, sunflower is first when the cultivation area and production are investigated. Approximately 50% of the vegetable oils produced in our country are obtained from sunflowers. There is a continuous increase in vegetable oil consumption in Türkiye because of both rapid population growth and increased consumption per capita (Onurlubaş & Kızılaslan, 2007).

Net Primary Productivity (NPP) is directly related to the yield of harvested product. NPP can be determined by the Light Use Efficiency (LUE) model with the help of remote sensing data. LUE models are widely used around the world to decide NPP for the assessment of global carbon cycle rates (Ahl et al., 2004; Olofsson et al., 2007; Drolet et al., 2008; Propastin et al., 2012; Wellington et al., 2022). The LUE approach is well suited to satellite-based NPP estimation, as plant radiation absorption is the main subject for net carbon production (Field et al., 1995; McCallum et al., 2009). Data obtained from satellites can be used in studies related to product efficiency, as they contain radiation emitted and reflected from the Earth at various wavelengths of the electromagnetic spectrum (Tao et al., 2005; Gitelson et al., 2012). While establishing the yield model, many different parameters are analyzed together. Meteorological parameters such as temperature, humidity, solar radiation, and soil conditions should be monitored throughout the plant phenology (Soltani et al., 2005; Bazgir et al., 2007; Algancı, 2014). Besides these parameters, spectral plant indices, widely used in mapping, monitoring, and analyzing temporal and spatial changes in plant structure and even some biophysical parameters, are also used in the yield model (Almalki et al., 2022). These indices are used in the yield model to monitor and evaluate changes in the biophysical properties of vegetation such as fPAR (photosynthetic active radiation absorption coefficient), leaf area index (LAI), and crop cover fraction (CCF) (Asrar et al., 1984; Holben, 1986; Myneni et al., 1995; Myneni et al., 1997a; Myneni et al., 1997b; Gitelson et al., 2002; Guo et al., 2018; Peng et al., 2019).

In yield estimation studies, LAI is used instead of the fPAR value(Qin et al., 2018; Algancı, 2014). LAI is one of the biophysical variables required for yield estimation. Direct LAI measurements are time-consuming and difficult. (Bréda, 2003). Devices for direct LAI measurements need to be calibrated precisely to the study area (Poblete-Echeverría et al. 2015). Therefore, instead of direct LAI measurements, the crop cover fraction, which is known to have a high correlation with LAI, is used in studies instead of LAI (Pan et al., 2007). High spatial is obtained at small spatial scales from ground-based methods, which traditional methods used in determining the crop cover fraction. However, it is time-consuming and labor-intensive with researcher subjectivity (Zhou et al., 1998; Richardson et al., 2001; Herrick et al., 2006; Poblete-Echeverría et al., 2015). With digital cameras, crop cover fractions can be obtained faster, more accessible, and more accurately. With image processing software, crop cover fraction information can be obtained by taking the percentage of the total number of pixels to the green pixels. In methods used to extract crop cover fraction from digital camera images (Dymond et al., 1992; Elvidge & Chen, 1995; Senseman et al., 1996; Purevdorj et al., 1998; Adamsen et al., 1999; Lukina et al., 1999; Elmore et al., 2000; Zhou & Robson, 2001; Pan et al., 2007), especially in RGB (Red, Green, Blue) images without near-infrared bands, it is very difficult to distinguish plant characteristics from each other in green, aged plant communities. Correlation between bands is high in RGB color space. However, this correlation between bands decreases when images are converted to HSI (hue-saturation-intensity) space. There are many studies where more accurate results are obtained from digital images used in plant analysis with HSI conversions rather than original RGB bands (Liu et al., 2012). In a study by (Tang et al., 2000), HSI conversion was made to high-resolution video images to detect weeds in the plant. (Ewing & Horton, 1999) used the HSI transformation to determine the wheat plant's crop cover fraction in their study. (Suarez Baron et al., 2022) and (Kaushalya Madhavi et al., 2022) used the HIS transformation to separate the leaf from the background. The second method used to determine the crop cover fraction is the GreenCrop Tracker software. Green Crop Tracker software is an alternative tool that assists researchers in processing digital color images under open-source licensing, which Agriculture and Agri-Food Canada use to obtain the crop cover fraction in agricultural areas and LAI value (Liu & Pattey, 2010). The GreenCrop Tracker's ease of use, cheapness, and the fact that it does not require on-site measurements like conventional LAI measurements reveal the advantages of this tool (Sandhu et al., 2018).

fPAR can be derived from remote sensing data due to the relationship between absorbed solar energy and spectral vegetation indices (Myneni et al., 1995; Yuan et al., 2007; Zhao et al., 2020). This relationship is usually made by applying Beer's law, which defines light absorption as the LAI factor (Running et al., 2004; Yuan et al., 2007). Studies show that fPAR is linearly related to the normalized difference vegetation index (NDVI) in different habitats (Yuan et al., 2007). In our study, the crop cover fraction was subjected to regression analysis with 12 vegetation indices NDVI, (green normalized difference vegetation index) GNDVI, (Soil-Adjusted Vegetation Index) SAVI, (difference vegetation index) DVI, (Ratio Vegetation Index) RVI, (Enhanced Vegetation Index)

EVI, (Generalized Difference Vegetation Index) GDVI, (green red vegetation index) GRVI, (Normalized Green) NG, (normalized NIR Index) NNIR, (Normalized Red) NR, (transformed soil-adjusted vegetation index) TSAVI) obtained from SPOT 6 and SPOT 7 satellite images. Regression analysis is a statistical technique used to examine the connections between variables. The investigator also commonly evaluates the "statistical significance" of the estimated relationships, which refers to the level of confidence that the genuine relationship is similar to the calculated relationship (Sykes,1993). The relationship between these vegetation indices and the crop cover fraction was investigated. The value of crop cover fraction obtained from NDVI and other vegetation indices was compared with the value of crop cover fraction obtained from pixel-based classification with RGB to HSI method, and crop cover fraction accepted with Green Crop Tracker software NDVI value was observed to have the highest correlation with the crop cover fraction in 3 years.

Pixel-based classification analysis is generally used to extract information from digital images. In this method, the digital value of each pixel is evaluated individually. In another technique, object-based image analysis, pixels are segmented into objects with homogeneous spectral and spatial properties (Ryherd & Woodcock, 1996). In the second step, these objects are classified instead of a single pixel. In ecological research, object-based classification analysis is very advantageous because it can determine the boundaries between species well (Hay et al., 2002). By applying HSI transformation to digital images in the calculation of crop cover fraction using image-based methods, crop cover fraction can be extracted with object-based classification (Ewing & Horton, 1999; Tang et al., 2000; Hemming & Rath, 2001; Laliberte et al., 2007; Karakus & Karabork, 2017).

Generally, when selecting satellite images, the cost and dimensions of the study area are considered. Satellites with a spatial resolution below 1m are defined as very high resolution, between 1m and 5m as high resolution, between 5m and 30m as medium resolution, and between 30 m and 300 m as low resolution. It is seen that more studies are carried out for product identification with low and medium-resolution satellite images (Huang et al., 2002; Hoberg & Müller, 2011; Leite et al., 2011; Peña-Barragánet al., 2011; Yang et al., 2011; Faria et al., 2012). The study investigated the effect of a 1.5-meter resolution SPOT 7 satellite image on yield estimation.

Although the method followed in yield estimation uses multi-time satellite images in general (Ines & Honda 2005; Algancı, 2014), the desired number of satellite images cannot be obtained due to many factors, such as cloud rate and low temporal resolution. It has been observed that the best estimation can be made with a single image taken during the bloom period, that is, during the pollination period (Lobell et al., 2003; Jongschaap, 2007). If we examine these studies more closely, in their research, (Lobell et al., 2003) estimated crop area, yield, and planting dates with Landsat images for 2 years in an intensive agriculture region in northwest Mexico. Crop phenology information was combined with multi-temporal satellite images to predict regional crop rotations. Appropriate sowing dates were determined to identify yield and wheat yield using NDVI and SR indices as fPAR. A simplified model was developed to assess the assassination of yield using only one image, and high accuracy was achieved based on the image acquisition date. Another study (Jongschaap, 2007) stated that if multiple photos cannot be obtained in yield estimation for various reasons, a very accurate yield estimation can be made with a single-dated image tried before harvesting. However, the effects of soil class on yield could not be modeled in these studies. In our research, while estimating the yield with a single satellite image, satellite image selection was made considering that different agricultural plants will be planted in the region and the difference in development rates and durations of these plants. While determining the single-dated images, the most suitable period was chosen by considering the development status between the same or recently cultivated species.

This study aims to develop the fields with the help of meteorological data and use a single satellite image every year in the Kadirli District of Osmaniye Province in Türkiye. The second aim is to examine the effect of the results obtained by adhering to the soil maps on the yield models. This study conducted a comprehensive field study to determine which crop was grown in which field in 2013, including the Kadirli-Osmaniye-Kozan districts, and to decide which products to work with. As a result of this field study, it was determined that most corn and sunflower plants were grown in the study area. Farmer interviews determined the planting harvest dates of these two plants. It was determined that the fields were irrigated, but the amount of water used per decare could not be determined because irrigation is done until the field reaches water saturation. In the years 2014-2015 and 2016, when the yield estimation will be made, plant height measurements and monitoring of plants started in April, when the crops sown were noticeable on the soil surface, such as late February - early March. Images were obtained from a 1-1.5 m height from the plant surface with the camera. Plant height measurements were provided until plant height growth ceased, and images were taken until the plant was harvested. Regression analysis was performed with 12 vegetation indexes obtained from satellite images and crop cover fractions. In all calculated yield models, the relationship between I.-II.-III. soil classes selected, considering soil maps and yield, are compared. The relative errors of the low-yield fields were calculated between 10% and 35% (according to the yields obtained at harvest time). As a result, it was determined that a single satellite image could model yield estimation of corn and sunflower for each year on fields with an average of 0.10 relative errors.

Material and Methods

Study Area

Kadirli, chosen as the study area, is located in the north of Osmaniye province in Türkiye and is the largest district of Osmaniye. One-third of the district's lands are mountainous, and two-thirds are plains. Therefore, Kadirli is a settlement whose economy is based on agriculture. The subtropical Mediterranean climate is dominant in Kadirli. Summers are dry, and winters are mild and rainy. The highest average temperature in the district is in August at 36 °C, the lowest temperature is in January with an average of 3 °C, and the annual average precipitation is 1,000 mm per m². Osmaniye has a green area above Türkiye and world standards, with its green areas and forests of up to 40% (Url-1). Due to all these features, the region has been chosen as the study area because it has the most suitable climate and soil for agriculture. Different characteristics, such as slopes and flat regions, were taken into account. In Fig. 1., I., II., and III. class lands, which belong to the study area, are represented.

In these test areas, sunflowers and corn were planted in early February or early March, depending on the hot or rainy weather and the location of the fields in 2014, 2015, and 2016. In this region, corn is generally planted in February if the weather is dry, and sunflowers are usually planted at the beginning of March.

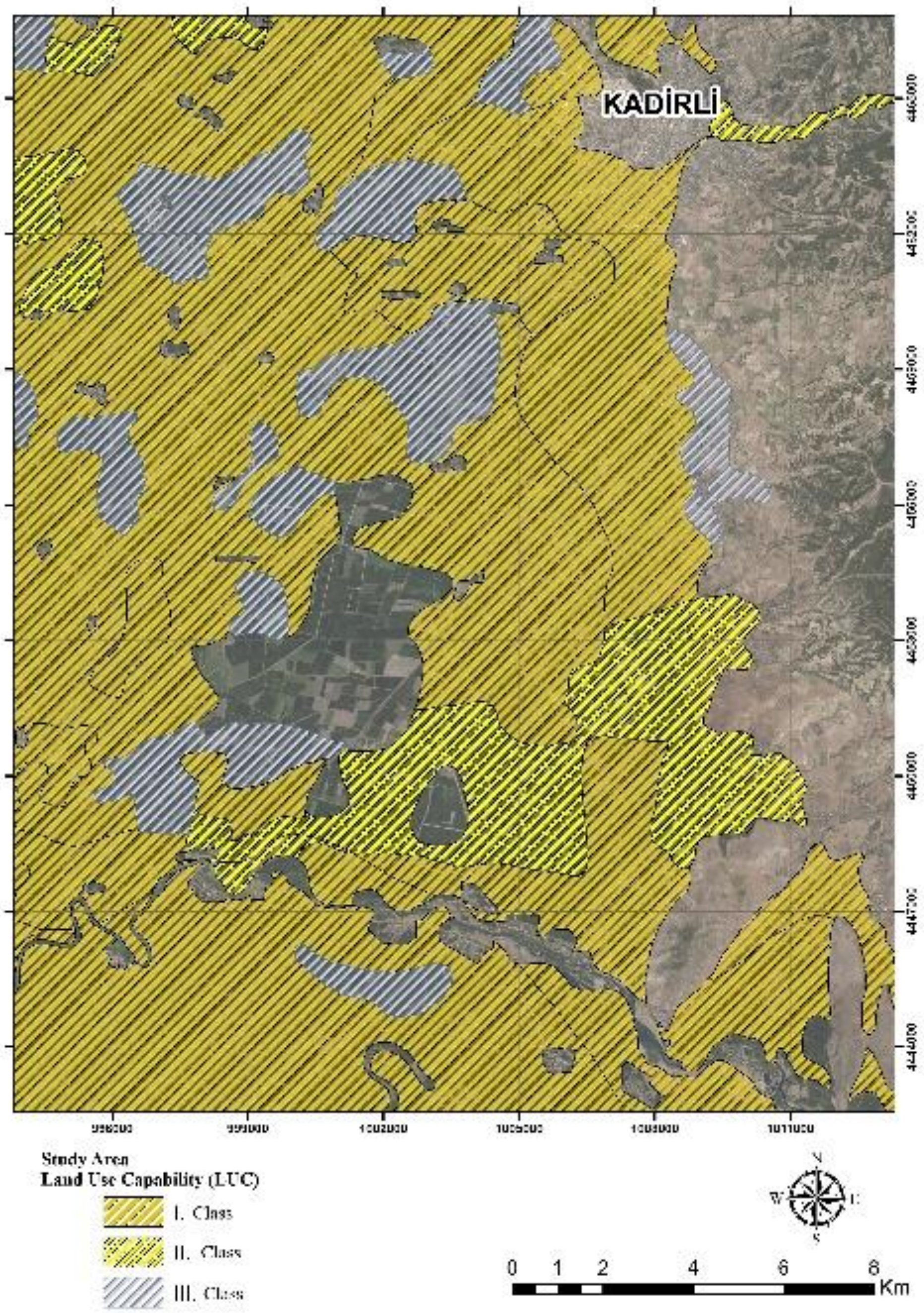

Fig. 1. Land use capability map of the study area

Selection of Test Cropland

To investigate the effect of soil classes on yield estimation, 1/100.000 scaled soil maps of the study area were examined. When all lands are examined in general, according to the Land Use Capability (LUC) in Türkiye, with the I. class, which can be cultivated in the best, easiest, and most economical way without causing erosion on the soil, and places that are not suitable for any agriculture, cannot be used even as meadow or forest, but only constitute an environment to the natural life or used by people as resting places and national park are situated among the VIII. class (Url-2). In this study, 4-5 cropland from each class land where corn and sunflowers are cultivated was tried to be selected in Fig 2, and the class lands are I. class land, where agriculture is more intensive, II. class land, and III. class land.

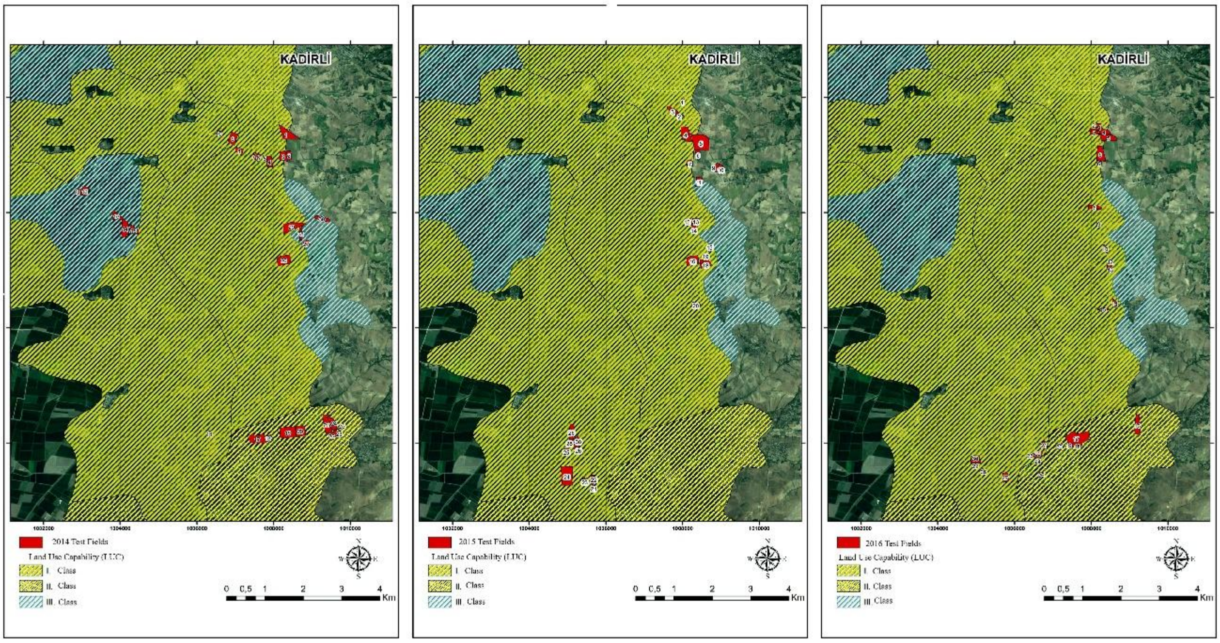

Fig.2. Selected test fields in 2014-2015-2016

Selection of Plant Species

The development period of the corn plant lasts 70-165 days. Although it varies according to the species and cultivated area, it requires a temperature of 10-13 °C during the germination period and 10-20 °C during the growth period (Türkoğlu, 1971). Corn is generally grown in humid and warm areas.

Although sunflower is not selective in the soil in which it grows, it can be grown with high yield in deep soils rich in organic matter and with good water-holding capacity. It can be grown in well-drained soils, from sandy to clay. Although sunflower is a very tolerant plant to high and low temperatures, a soil temperature of 8-10 ℃ is required for the best germination of its seeds. The best-growing temperatures for sunflowers are between 21 ℃ and 24 ℃ (Türkoğlu, 1971).

Satellite data and image processing

In the study, SPOT 6 & SPOT 7 satellite images were used. On June 10, 2014, and July 13, 2015, 6 meters resolution (Ground Sampling Distance – GSD) for blue, green, red, and near-infrared channels in multispectral detection mode, and on June 2, 2016, 1.5 meters resolution pan-sharpened blue, green, red, and near-infrared band data have been provided as shown in Tab. 1.

Tab. 1. SPOT 6 and SPOT 7 properties

SPOT 6	***Bands***	***GSD***	***SPOT 7***	***Bands***	***GSD (pan-sharpened)***
Blue	*0.45-0.52 µm*	*6 m.*	*Blue*	*0.45-0.52 µm*	*1.5 m.*
Green	*0.53-060 µm*	*6 m.*	*Green*	*0.53-060 µm*	*1.5 m.*
Red	*0.62-0.69 µm*	*6 m.*	*Red*	*0.62-0.69 µm*	*1.5 m.*
NIR	*0.76-0.89 µm*	*6 m.*	*NIR*	*0.76-0.89 µm*	*1.5 m.*

In this study, atmospheric and geometric corrections on satellite images were made using ENVI software. The QUick Atmospheric Correction (QUAC) method directly determines the atmospheric correction parameters from the observed pixel spectrum in an image without additional information. QUAC results are better than FLAASH or other physics-based first-order methods (Bernstein et al., 2012). For this reason, atmospheric correction of satellite images was made with QUAC in the study.

The 16 control points required for the geometric transformation of the image were obtained with RTK-GPS. It is received within a 0.5-pixel error limit using first-order polynomial transformation with the help of ground control points.

Meteorological Data Processing

The meteorological parameters of daily solar radiation, such as daily minimum, daily maximum, average temperature, and daily average wind speed, required in the LUE model were obtained from TARBIL. Fifteen meteorological stations near Kadirli, shown in Fig. 3, have been determined to be used in the study. The minimum, maximum, and average temperature values were used to calculate the meteorological data for 2014, 2015, and 2016.

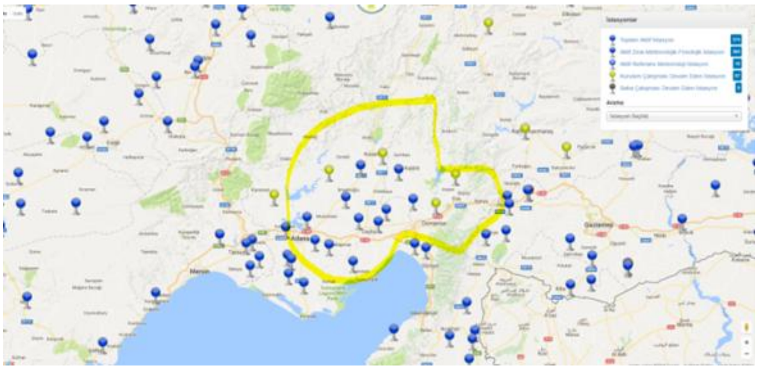

Fig.3. Meteorological stations around Kadirli district

The LUE model and its parameterization

Production efficiency estimation is based on a concept developed by (Monteith, 1972; Monteith, 1977). This concept suggests that crop productivity is related to fPAR, PAR, and LUE (Hall et al., 1992; Viña and Gitelson, 2005). NPP is calculated using the equations in (1 and 3).

$$NPP = LUE \times fPAR \times PAR \tag{1}$$

$$LUE = \varepsilon_0 * T_s * SM \tag{2}$$

$$NPP = \varepsilon_0 * fPAR * PAR * T_s * SM \tag{3}$$

PAR is accepted to be 45-50% of solar radiation data. PAR is calculated from solar radiation data (Bastiaanssen & Ali, 2003).

Another parameter used in LUE yield models is the harvest index parameter. Harvest index parameters defined as grain moisture content (mm) (MC), harvest index (grain/stalk ratio) (HI), and root-stem weight ratio (AL) for corn and sunflower are determined by local measurements and experimental studies in a laboratory environment. Since there are no terrestrial measurements, the literature (Anderson, 1988; Dwyer et al., 1994; Algancı, 2014) determined these parameters by interviews with the farmer, as seen in Tab. 2.

Tab. 2. Harvest index parameters for sunflower and corn.

SPOT 6	Sunflower	Corn
HI (%)	0.20-0.35	0.40-0.55
KGO (%)	0.30	0.70-0.85
NO (%)	0.20	0-0.20

The value represented as ε_0 found in the LUE yield model is considered relatively constant during the phenological period, provided that the climatic conditions are good and the soil is adequately irrigated (Monteith, 1972).

$$LUE = \varepsilon_0 * T_s * SM \tag{4}$$

$\varepsilon_0 = 0{,}389\ gCm^{-2}MJ^{-1}\ APAR$ is taken as such (Potter et al., 1993).

While $\boldsymbol{\varepsilon_0}$ found in equation (4) expresses the maximum LUE value, $\boldsymbol{T_s}$ expresses the temperature influence factor, and SM stands for soil moisture. A detailed literature review on the effect of temperature on corn and sunflower production was made, and it was calculated with equation (4) (Yuan et al., 2007; Barr et al., 2013; Kross et al., 2016; Yuan et al., 2016).

$$T_S = \frac{(T - T_{min})(T - T_{max})}{[(T - T_{min})(T - T_{max})] - (T - T_{opt})^2} \tag{5}$$

T_{min},T_{max}, T_{opt} are temperatures at which the photosynthesis activities of the plant are minimum, maximum, and optimum. On the other hand, T is the average daily air temperature. If the air temperature is below T_{min} or above T_{max}, T_S= 0 (Raich et al., 1991). T_S "The temperature effect coefficient" differs according to the species and the region it lives in. The temperature effect coefficient takes a value between 0 and 1. Root elongation of the corn plant in our study area stops below 9 °C, and there is a sudden decrease in root and stem elongation when it reaches 32 °C, and stomal activities stop completely at 40 °C as seen in Fig. 4 (Kırtok, 1998). As seen in Fig. 4, root elongation stops below 10°C for sunflower, a sudden decrease in root and stem elongation is observed when it reaches 35 °C, and stomal activities stop completely at 45 °C (Gürbüz et al., 2003). The temperature effect factor values calculated for corn and sunflower according to equation (5) are shown in Tab. 3.

Tab. 3. The effect of temperature on corn and sunflower

Date	Sunflower soil moisture index	Corn soil moisture index
2014	0.92	0.92
2015	1	1
2016	0.9168	0.9168

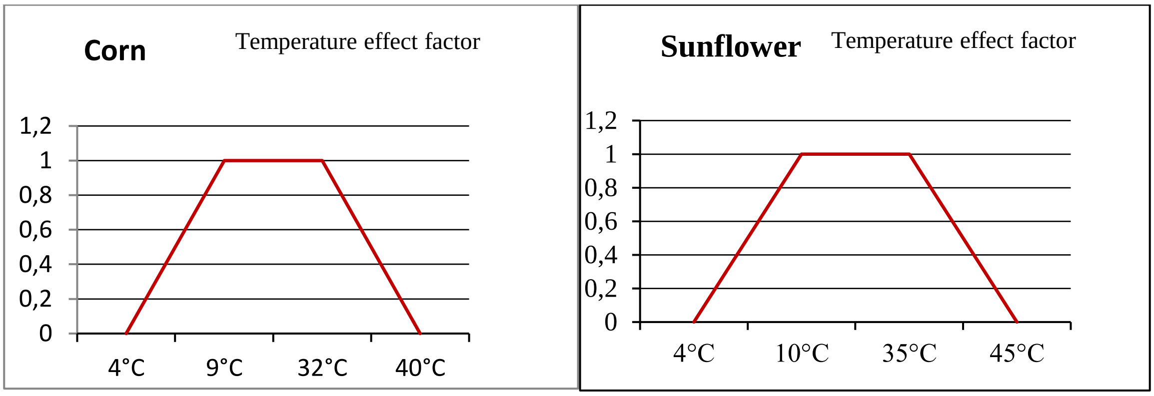

Fig. 4. T_S for corn and sunflower

Soil moisture index is calculated with $W = 0{,}5 + 0{,}5 * (ET/PET)$. ET is evaporation, and PET is potential evaporation. AgroMetShell plant climate model, an FAO software, was used to calculate ET and PET values using the FAO-Penman-Monteith method. The climatic data required for the technique include temperature (maximum and minimum values), global solar radiation or sunshine duration, and average wind speed (Tao et al., 2003). The soil moisture index values obtained with the AgroMetShell plant climate model are shown in Tab. 4.

Tab. 4. Soil moisture index values of corn and sunflower

Date	Sunflower	Corn
2014	1	1
2015	1	0.8616
2016	1	1

Another parameter required for yield estimation is photosynthetically active radiation (PAR) (0.4-0.7 µm). This parameter is described as a portion of the short-wave solar radiation (0.3-3 µm) absorbed by chlorophyll, which is necessary for plant photosynthesis. This parameter can be obtained from meteorological data sets and satellite data (Dye & Shibasaki, 1995). PAR is the K fraction of incoming solar radiation. PAR is considered to be

45-50% of the average 24-hour solar radiation. K↓expresses the value of space radiation (Moran et al., 1995; Bastiaanssen & Ali, 2003). Tab. 5 shows the PAR values calculated for 2014, 2015, and 2016 with equality (6).

$$PAR = 0{,}48 * K(W\ m^{-2}) = \text{MJ}\ m^{-2} day^{-1} \quad (6)$$

Tab.5. PAR values of corn and sunflower

Date	*Sunflower PAR [$MJm^{-2}day^{-1}$]*	*Corn PAR [$MJm^{-2}day^{-1}$]*
2014	*11.3173314*	*11.3173314*
2015	*12.27865651*	*12.27865651*
2016	*12.0589503*	*12.0589503*

fPAR refers to the portion of available PAR that plants can absorb for carbon sequestration. This value varies according to the type of plant and growing conditions. This value is closely related to vegetation indices (Baret et al., 2007; Houborg et al., 2011; Bandaru et al., 2013). The fPAR value used in yield estimation was determined by two methods in this study. The first is the linear relationship between fPAR and vegetation indices using remote sensing methods. The vegetation indices that best match the crop cover fraction to be used in yield estimation by (Jones & Vaughan, 2010) are explained below.

NDVI is directly proportional to the amount of chlorophyll in the plant and is used to determine its health status (Rouse, 1974).

NDVI=(NIR-Red)/(NIR+Red)
NIR: Reflectance values detected at Near Infrared wavelengths
Red: Reflectance values detected at Red wavelengths

GNDVI is an improved form of NDVI that is more sensitive to the diversity of chlorophyll content in the plant (Gitelson et al., 1996).

GNDVI=(NIR-Green)/(NIR+Green)
NIR: Reflectance values detected at Near Infrared wavelengths
Green: Reflectance values detected at Green wavelengths

Unlike NDVI, SAVI is a vegetation index calculated by considering the reflection of the soil (Huete, 1988).

SAVI=(1+L)(NIR-Red)/(NIR+Red+L)
L= Soil brightness factor
NIR: Reflectance values detected at Near Infrared wavelengths
Red: Reflectance values detected at Red wavelengths

DVI is used to distinguish soil and vegetation.
DVI=(NIR-Red)
NIR: Reflectance values detected at Near Infrared wavelengths
Red: Reflectance values detected at Red wavelengths

RVI is also used to determine vegetation.
RVI=(NIR/Red)
NIR: Reflectance values detected at Near Infrared wavelengths
Red: Reflectance values detected at Red wavelengths

NDVI is more sensitive to changes in high-mass areas, which is a major shortcoming of NDVI. EVI is a vegetation index that reduces the effect of atmospheric conditions (Liu and Huete, 1995).
EVI=G * [(NIR – red) / (NIR + C1*Red – C2*Blue + L)],
G = 2.5, C1 = 6, C2 = 7.5, L = 1
NIR: Reflectance values detected at Near Infrared wavelengths
Red: Reflectance values detected at Red wavelengths
Blue: Reflectance values detected at Blue wavelengths

GDVI is a plant index developed to determine the nitrogen need in corn plants (Sripada et al., 2006).
GDVI=(NIR-Green)
NIR: Reflectance values detected at Near Infrared wavelengths

Green: Reflectance values detected at Red wavelengths

GRVI is strongly affected by the green and red reflection changes that occur in the pigments in the leaf (Sripada et al., 2006).

GRVI=(NIR/Green)

NIR: Reflectance values detected at Near Infrared wavelengths

Green: Reflectance values detected at Red wavelengths

Since NG is sensitive to pigments other than chlorophyll (carotenoids, anthocyanins, xanthophylls) found in the plant, it is used to determine these pigments in the plant (Sripada et al., 2006).

NG=Green/(NIR+Red+Green)

NIR: Reflectance values detected at Near Infrared wavelengths

Red: Reflectance values detected at Red wavelengths

Green: Reflectance values detected at Green wavelengths

Since NNIR is sensitive to the chlorophyll content in the plant, it is used to determine the chlorophyll in plants (Sripada et al., 2006).

NNIR=NIR/(NIR+Red+Green)

NIR: Reflectance values detected at Near Infrared wavelengths

Red: Reflectance values detected at Red wavelengths

Green: Reflectance values detected at Green wavelengths

NR is used to determine the chlorophyll content in the plant (Sripada et al., 2006).

NR=Red/(NIR+Red+Green)

NIR: Reflectance values detected at Near Infrared wavelengths

Red: Reflectance values detected at Red wavelengths

Green: Reflectance values detected at Green wavelengths

The soil effect is tried to be minimized with a slope, b soil intersections and X coefficient values in TSAVI (Baret et al., 1989).

$$TSAVI = [a\ (NIR - a*Red - b)] / [a*NIR + Red - (a*b) + X(1+a^2)]\ ;$$

a=1.2 , b=0.04, 38 X=0.8 constants.

NIR: Reflectance values detected at Near Infrared wavelengths

Red: Reflectance values detected at Red wavelengths

This study used vegetation indices such as NDVI, GNDVI, SAVI, DVI, RVI, EVI, GDVI, GRVI, NG, NNIR, NR, and TSAVI. For sunflower and corn, a regression was calculated between the vegetation indices and crop cover fraction on a parcel basis. Among all these indices, the NDVI value gave higher correlation values than the other indices. Studies also show that the NDVI value is linearly related to fPAR (Prince & Goward, 1995; Goetz & Prince, 1999; Lobell et al., 2003). Some studies explain these relations(Sala & Paruelo, 1997; Seaquist et al., 2003; Url-3)

Another method used in this study to calculate the fPAR value is digital images. The crop cover fraction will be used instead of the FPAR value in the yield model. The digital images used in this study were obtained with the Sony DSC-S930 camera. The camera has a focal length ranging from 6.4 to 19.2 mm. Its sensor is 10 megapixels in resolution. Image dimensions are a maximum of 3648x2736 pixels, weighing 167 grams. It was paid attention to keep the zoom setting the same during the photoshoots that took 3 years. The focal length was taken as 6.4 mm in all images. The photos were taken from 1-1.5 m height with automatic exposure facing vertically down in the plots. Images and plant height measurements were taken every week throughout the plants' growing period. The purpose of taking these digital photographs is to define the crop cover fraction of sunflowers and corn during their growing stages. Crop cover fraction expresses the percentage of the plant (including roots, branches, and leaves) in the total area of interest to the vertical projection area (Purevdorj et al., 1998; Gitelson et al., 2002; Godínez-Alvarez et al., 2009). Crop cover fraction is a biophysical variable important in carbon cycle studies(Xiao et al., 2016). This study used two methods to determine the crop cover fraction. The first is converting the RGB image space to the HSI color space. RGB color representation is based on a cube, whereas HSI is based on a color sphere (Jensen, 2005). Intensity is related to brightness. This value indicates the vertical axis of the sphere. The hue describes the dominant wavelength of the color. This value indicates the circumference of the sphere. Another value saturation is the relative purity of the color. This value describes the radius of the sphere. While hue and saturation values are related to people's ability to perceive colors, the HSI model is separated from color information by the intensity component. In this method, RGB values can be easily transferred to HSI values, as seen in the equations (7, 8, 9). In the HSI color space, the hue of color describes an angle. It also has a relationship with the closest matching spectral wavelength. The hue ranges from 0° to 240° in the visible spectrum and can optionally be red hue at 0°, green hue at 120° and blue hue at 240°. Between 240° and 360°, there are colors that the eye cannot perceive (Pan et al., 2007). The conversion from RGB to HSI is as shown below(Li et al.,2002):

$$I = \frac{1}{3}(R + G + B) \tag{7}$$

$$S = 1 - \frac{3 \times min\ (R, G, B)}{R + G + B} \tag{8}$$

$$H = cos^{-1}\left[\frac{1/2((R - G) + (R - B))}{\sqrt{(R - G)^2 + (R - B)(G - B)}}\right] \tag{9}$$

Here, R=Red, G=Green, and B=Blue in the RGB color space. If G ≥ B, then H = 360 - H; if R = G = B, then H is undefined and S = 0 (Pan et al., 2007). In the present study, RGB images were first converted to HSI. Then, object-based classification was used to distinguish the plant from the soil surface. The images were segmented by selecting the appropriate parameters. Plant and non-plant parts were identified and classified using control data. The crop cover fraction was then obtained by dividing the number of green pixels of the plant by the total number of pixels. Fig. 5 shows the conversion of field 23 of 2014 from RGB to HSI.

Fig.5. HSI representation of field number 23 in 2014

The second method used to determine the crop cover fraction is Green Crop Tracker v.1.0 software developed by Agriculture and Agri-Food Canada (Liu & Pattey, 2010). This software is freely available and calculates the crop cover fraction from color images in coordination with IDL (Interactive Data Language). The software uses red(R), green(G), and blue(B) values, as seen in equation (10).

$$Greenness = 2G - B - R \tag{10}$$

The R, G, and B values here are the intensity levels for each color. These values are obtained with a digital camera. The formulation is based on a high contrast between the reflected intensity of green leaves and the other background colors associated with features such as soil, dry leaves, etc. This software calculates the crop cover fraction with the sequential threshold value approach based on histogram analysis (Liu & Pattey, 2010).

Yield estimation with a single date

In cases where it is not possible to work with multiple satellite images due to limitations such as the cost of satellite imagery and the presence of clouds in the study area, it is very important to choose the most appropriate time for yield estimations with a single satellite image. Yield estimation was made by taking satellite images from June 10, 2014, July 13, 2015, and June 2, 2016, when the green of plants was the most intense. NDVI values were calculated from the satellite images taken on these dates and used in yield estimation models.

Results and Discussion

Crop cover fraction

Corn number 4 in 2014, sunflower number 6 in 2014, sunflower number 14 in 2015, the chart of corn numbered 15 in 2015 that was used to calculate the crop cover fraction of the fields of corn number 18 in 2016 and sunflower number 29 in 2016 by two methods and date graph number. The plant height date chart that determined the plant phenology is given in Fig. 6-7-8. As can be seen in the figures, it gives very close results. However, it has been observed that the images taken with the Green Crop Tracker tool in low-light conditions need to be corrected in the crop cover fraction. However, it was concluded that the Green Crop Tracker tool could quickly determine the crop cover fraction. At the same time, images used to calculate the crop cover fraction gave information about measured plant heights, plant phenologies, and plant diseases. Previous studies have shown that the GreenCrop Tracker can accurately predict CCF throughout the growth period of the crop, excluding the leaf aging stage (Sandhu et al., 2019; Karakus & Karabörk, 2020). The study by Karakus & Karabörk (2020) concluded that the Green Crop Tracker is a viable alternative to ground-based methods. In this approach, time and labor loss are less than in object-based classification. Green Crop Tracker software and object-based classification results were compared in growing seasons, and it was seen that a high correlation was obtained between these two methods, as in our study.

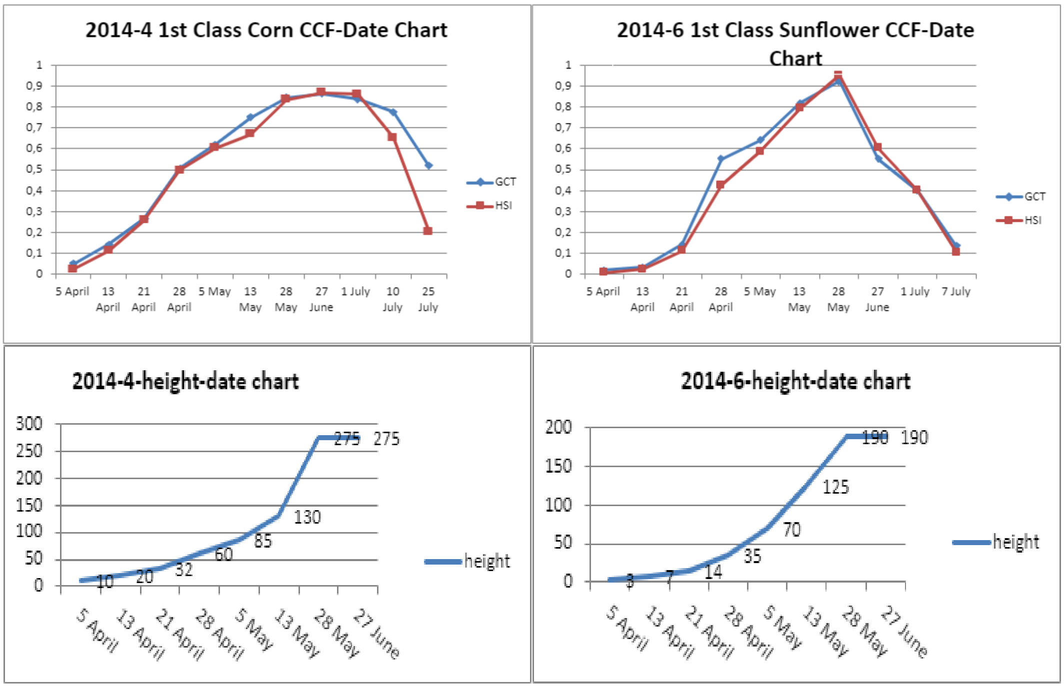

Fig. 6. The plant height-date that the plant phenology was determined for 2014 on corn and sunflower.

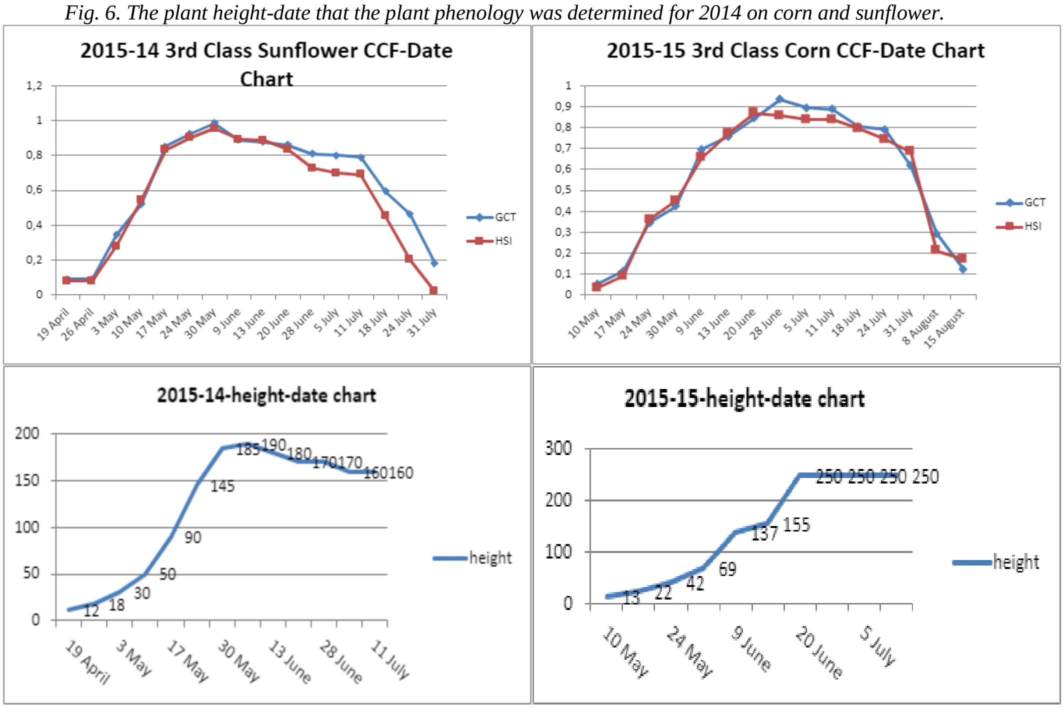

Fig. 7. The plant height-date that the plant phenology was determined for 2015 on corn and sunflower.

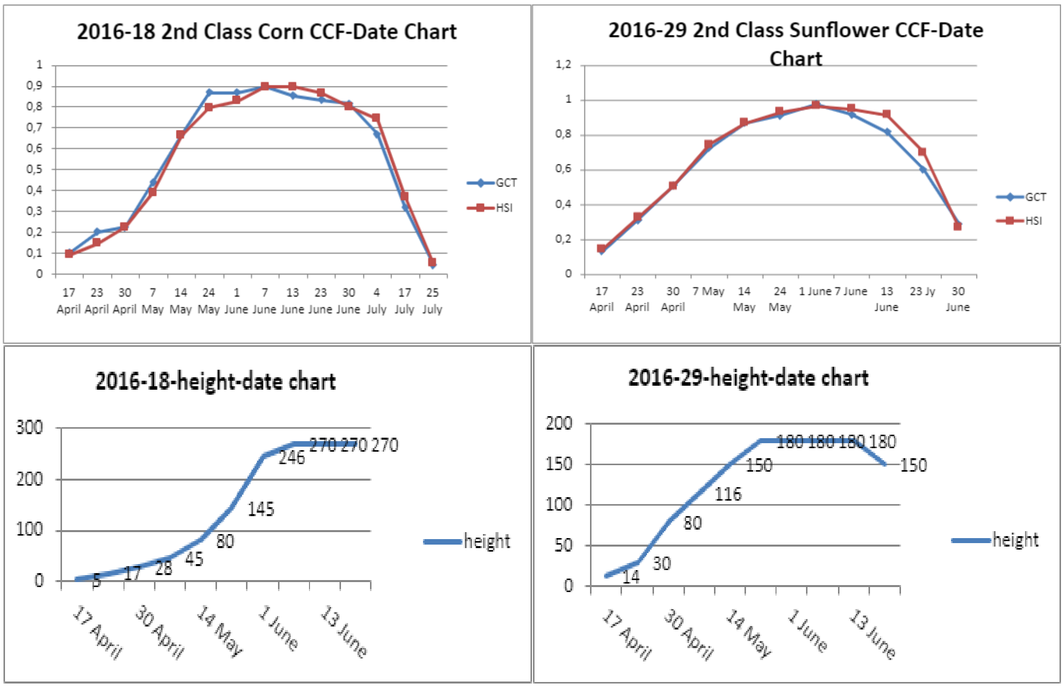

Fig. 8. The plant height-date of the plant phenology was determined for 2016 for corn and sunflower.

Relationship between vegetation indices and crop cover fraction

When regression was done between the vegetation indices of NDVI, GNDVI, SAVI, DVI, RVI, EVI, GDVI, GRVI, NG, NNIR, NR, and TSAVI on fields basis for sunflower and corn and crop cover fraction, NDVI gave higher correlation results between crop cover fraction and spectral vegetation indices. (Li et al., 2010) We also found a correlation of more than 0.86 between CCF and NDVI, which is parallel to our results. According to the results, the correlation is thought to increase due to the linear relationship between the NDVI and the crop cover fraction. For this reason, NDVI was used as the plant index in the presented study. At the same time, using NDVI-CCF correlations will contribute to standardizing the main approaches used to assimilate CCF into crop modeling applications (Jin et al., 2020). The results of linear regression analysis between NDVI-CCF were observed to have values between 0.710-0.907 R^2. NDVI- CCF equations and R^2 values, which were subjected to regression analysis in 2 groups, sunflower, and corn, are given in Tab. 6.

Tab. 6. CCF-NDVI equations for 2014, 2015 and 2016

Crop	***Date***	***Regression Equations***	***R²***
	2014	*CCF= -0.144 +1,113*NDVI*	*0.710*
Sunflower	*2015*	*CCF=0.007+1,030*NDVI*	*0.727*
	2016	*CCF= 0.102+0,853*NDVI*	*0.907*
	2014	*CCF= -0.061+1,073*NDVI*	*0.888*
Corn	*2015*	*CCF=0.046+0,951*NDVI*	*0.799*
	2016	*CCF=0.014+0,974*NDVI*	*0.834*

Results of yield estimation by years

Satellite images and crop cover fraction data were compared with farmer statements to verify yield estimates on a parcel basis. The satellite image taken in the field in 2014 fully reflects the vegetation density. Leaf manure was applied to fields 5 and 6 from the fields in 2014, and the highest yield was obtained. The yield is quite high since these fields are in the I. region. When the NDVI values and crop cover fraction values of these fields are examined, they are pretty high compared to other fields. In ll. field number 17 in the region, red spider disease was detected with the pictures taken on May 5 and the farmer interviews. This field's NDVI value and crop cover fraction are also the lowest compared to other cornfields. The relative error of field 17, in which red spider disease was detected, was high in all yield models. The last yield was obtained in the sunflower field number 27. Its NDVI values and crop cover fraction values are also relatively low. On the other hand, in field 27, where the lowest yield

was obtained, the relative error was found to be relatively high in all yield models. However, no signs of disease could be detected.
In 2015, it was determined that there was a water cut in corn number 30 on 13.6.2015 with field studies and farmer interviews. While it is thought to affect the yield, after 2 weeks, the yield was obtained above the expected with the fertilizer application. Crop cover fraction value also decreased after water cutting and increased after fertilization. A new seed was tried in field number 20, and the yield was at the expected level because it was in the I. region. A very high yield was obtained from pioneer seeds in fields numbered 3 and 14. The field, whose number is 3, is located in the I. region and has a higher NDVI value than other sunflowers in its region. Although the field number 14 is in the III. region, its NDVI value is 0.7999, which is relatively high compared to other sunflowers due to the newly tried seed. The relative error of all yield models needs to be corrected in field 4, where the yield is low. The relative error of the 14. field, which has the highest yield among all the Class III yield models, was also increased. Although the water cut disease was determined in field number 30, fertilization did not affect the yield in the appropriate period.
"Orhanbaş" disease occurred in the sunflower field number 4 in 2016. The lowest yield was obtained. NDVI and crop cover fraction are also very low, although it is a field in the I. Region.
As a result, it was seen that the land class gave results directly proportional to the yield in all yield estimation models (Tab. 7). However, low yields were observed in Class I fields in exceptional cases such as disease.

Tab. 7. Relative error results for sunflower and maize for 4 models

Model 1	*Sunflower*	*Corn*
2014	*0.114*	*0.101*
2015	*0.101*	*0.120*
2016	*0.103*	*0.107*
The mean of Model 1	*0.106*	*0.109*
Model 2		
2014	*0.098*	*0.087*
2015	*0.078*	*0.060*
2016	*0.088*	*0.089*
The mean of Model 2	*0.088*	*0.079*
Model 3		
2014	*0.117*	*0.096*
2015	*0.123*	*0.105*
2016	*0.088*	*0.124*
The mean of Model 3	*0.109*	*0.108*
Model 4		
2014	*0.097*	*0.080*
2015	*0.060*	*0.071*
2016	*0.088*	*0.089*
The mean of Model 4	*0.082*	*0.080*

It has been determined that the rainy weather in the tassel period in 2016 increased the crop yield a little compared to 2015. Because the temperature was above the seasonal normal, the corn sown in 2014-2016 was harvested on irrigated and uneven lands at the beginning of July. Another reason why the yield was better in 2016 compared to other years is the precipitation of corn in the formation of internal milk.

In Model 1 (fPAR=NDVI), fPAR is calculated from the NDVI calculated when the satellite image was taken. In Model 2 (fPAR=CCF) from the CCF extracted from the camera images at the time the satellite image was taken (as the LUE model is a daily model, the parameters need to be calculated daily. CCF values obtained from weekly camera images were converted to daily data by linear interpolation) were calculated from the NDVI calculated with other equations in the literature in the Model 3 (fPAR=1,24*NDVI-0,228), and from the equations derived from the relationship between the CCF and NDVI in the Model 4.

When the 4 yield models used in the study were examined, it was determined that the model in which fPAR=1.24*NDVI-0.228 was used as the fPAR value was not compatible with the field data and could not be used in yield estimation for this study. It was seen that the other 3 yield models were compatible with the field data.

The main reason for this was that Yield Model 3 was calculated using the equation used in the fPAR calculation from the literature, and it was not compatible with the field data, as it reflected the data of another study area. Among all yield models, lower relative errors were obtained for sunflower and corn plants in the yield model calculated with NDVI, which was obtained from the relationship between fPAR value, NDVI, and CCF.

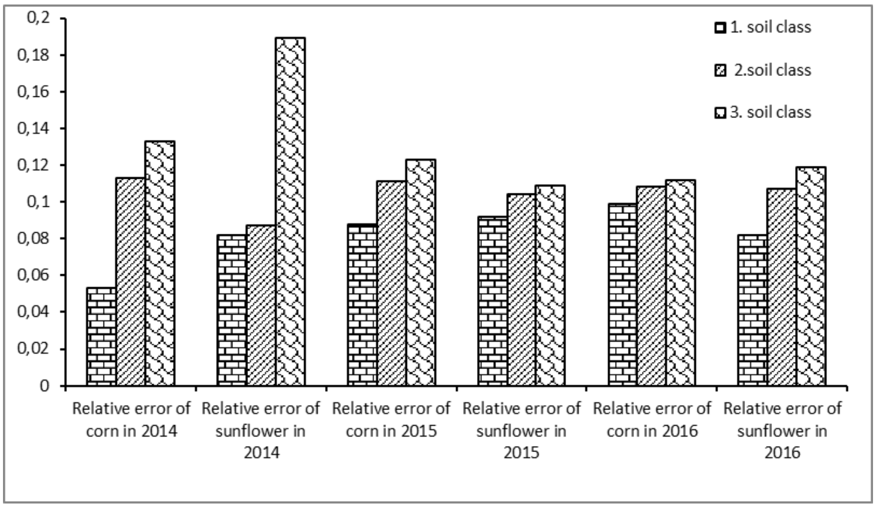

Fig. 9. Relative errors of 2014, 2015, and 2016 by soil class for yield model 1

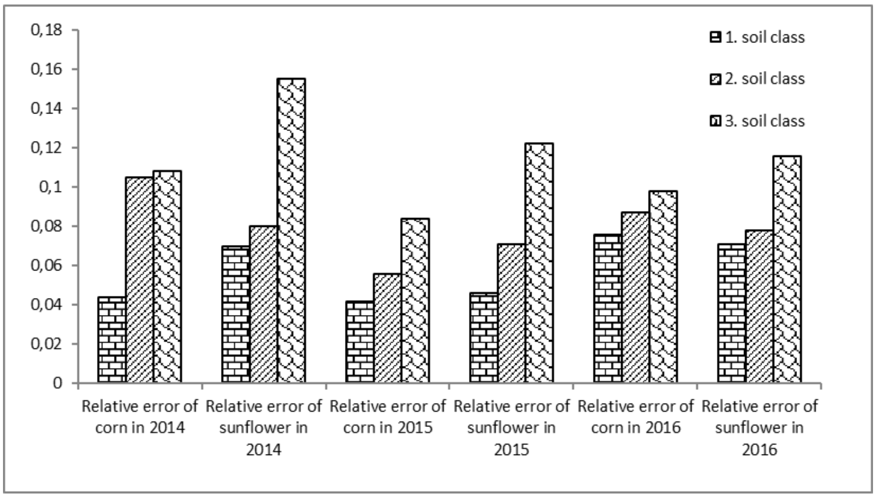

Fig.10. Relative errors of 2014, 2015, and 2016 by soil class for yield Model 2

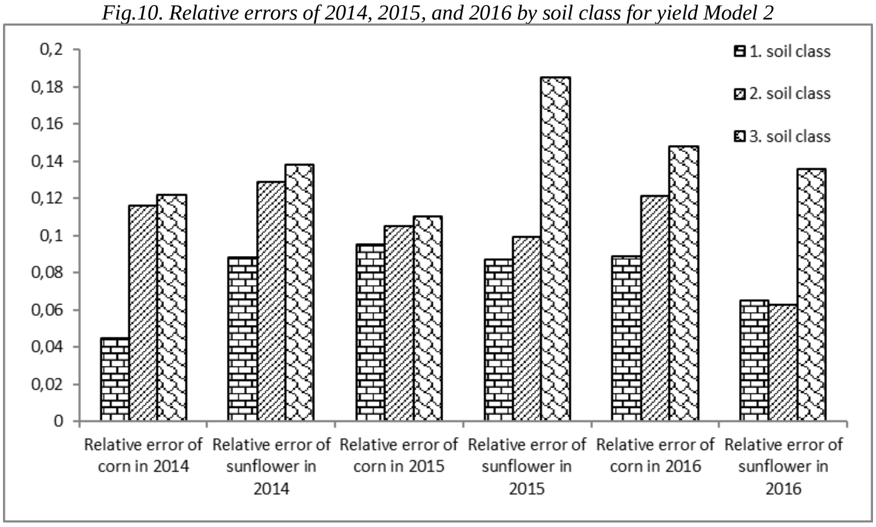

Fig. 11. Relative errors of 2014, 2015, and 2016 by soil class for yield Model 3

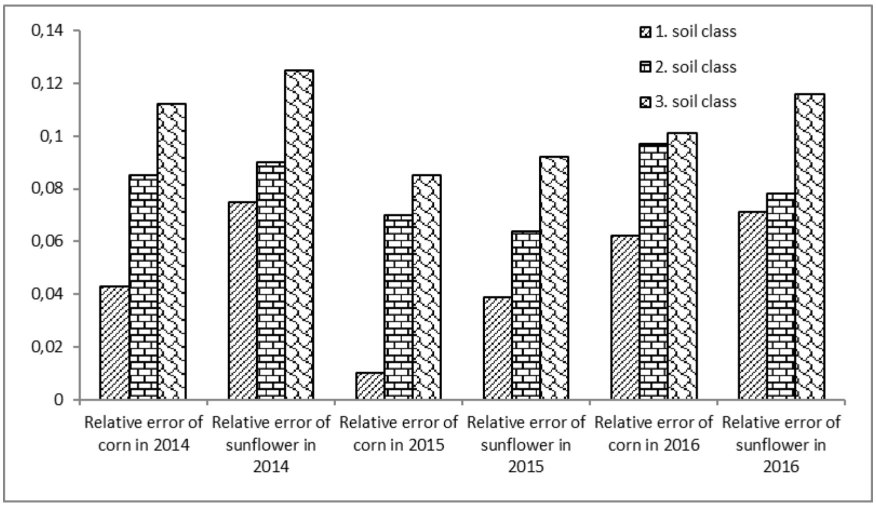

Fig. 12. Relative errors of 2014, 2015, and 2016 by soil class for yield Model 4

As a result, this model based on the fPAR approach with a single-dated satellite image and crop cover fraction obtained from camera images gave very effective results. The estimation accuracy of the model results established from the relationship between NDVI and crop cover fraction and the model results established from the crop cover fraction were calculated within 10% relative error. In the model using NDVI data directly as fPAR, relative errors for corn and sunflower were calculated above 10%.Similar to our study, it was seen in studies in the literature that more accurate yield estimation was made with Model 1 (He et al., 2018; Yuan et al., 2016). As stated by (Alganci et al., 2014), Model 2 obtained by taking CCF data instead of fPAR has achieved very successful results in yield estimation. (Alganc, 2014) concluded in another study that the yield estimation performance of Model 4 is better than that of Model 2 (Tab. 7). However, the effect of yield on soil class could be modeled in all yield models except Yield Model 3, which did not reflect the whole study area and data, and data compatible with the land data were obtained. Since the yield model 3 was calculated with the equation used in fPAR calculation from the literature and reflects the data of another study area, it was determined that it did not comply with the field data. In addition, if the yield model calculated with a single dated satellite image is compared with Yield Model 1, Yield Model 2, and Yield Model 4, it is seen that there is a 0.01% difference in the relative error. Considering the difficulty of classical terrestrial survey studies and the cost of working with multiple satellite images, very effective results were obtained.

When all methods performed in 2014, 2015, and 2016 about the effect of soil class on yield were analyzed on a parcel basis, an average relative error rate was determined with the relative error of 0.05 on average for corn and 0.05 to 0.100 for sunflower on 1. class lands, 0.100 to 0.150 for corn and sunflower in 2. class lands, and 0.100 and 0.200 in 3. Class lands. It was determined that there is a linear relationship between land classes and yield, as shown in Fig. 9-12. Yield models were calculated with a single satellite image taken at the most appropriate date and verified for 3 years recursively.

In the literature, yield estimation can be made often and accurately with multi-satellite imagery (Ines & Honda, 2005). On the other hand, yield estimation studies with a single satellite image are very limited. The studies did not consider the effect of soil classes on the yield model (Lobell et al., 2003). Within the scope of this study, yield estimations of corn and sunflower plants were made with high accuracy by including soil classes in the model.

Conclusions

In this study, it was seen that the yield estimation made with a single satellite image taken at the peak of vegetation can be made entirely accurate by following the phenological cycle of the product for which yield estimation will be made. With the plant pictures taken every week, plant height measurements, and farmer interviews, the plants' disease status, irrigation, and fertilizer application status were followed, and real-time ground reference information was provided. The GCT tool and the object-based classification method, which converts RGB to HSI, were used to determine the CCF added to the yield estimation model. It was determined that the CCF values obtained by these two methods were generally compatible. However, the CCF value obtained from the camera image of field 11 in 2014 due to the negative effect of illumination with the GCT tool on June 27 was calculated as 0.792, while the vegetation section value, which was converted from RGB to HSI and determined by object-based classification, was calculated as 0.918. It was analyzed that this difference was due to the low performance of the segmentation algorithm of the GCT tool and its insufficiency against the illumination conditions. For this reason, the method that converts RGB values to HSI values was used.

In this study, LUE-based yield models were tested. While determining the yield model, yield estimation was made in the fertile lands where corn and sunflower are planted in the Osmaniye Kadirli region, where agriculture is intensively done, with satellite images dated 2014, 2015, and 2016. To calculate the LUE yield model, fPAR, PAR, temperature, and soil moisture index parameters were determined. To determine these parameters, the average value method was used to spread the meteorological data (daily minimum temperature, daily maximum temperature, daily solar radiation, daily average wind speed, etc.). NDVI, vegetation section data, and meteorological data obtained from satellite images and yield estimates made on a parcel basis in 2014, 2015, and 2016 were compared with the yield values obtained by farmer declarations. At the end of this comparison, the mean relative errors of sunflower and corn plants as I, II, and III classes were calculated. For the corn plant, an average of 0.101 relative error was calculated in yield model 1, which was established with 2014 data, an average of 0.087 relative errors in yield model 2, an average of 0.096 relative errors in yield model 3, and an average of 0.080 relative errors in yield model 4. When the results of all yield models were analyzed on a parcel basis, it was seen that the models except yield model 3 were compatible with the field data.

In the literature, yield estimation can be made quite frequently and accurately with multiple satellite images (Ines & Honda, 2005). On the other hand, yield prediction studies using a single satellite image are quite limited. In the studies conducted, the effect of soil classes on the yield model was not taken into account (Lobell et al., 2003). Within the scope of this thesis, yield predictions of corn and sunflower plants were made with high accuracy by including soil classes in the model. It was determined that there was a linear relationship between land classes and yield. Yield models were calculated with a single satellite image taken on the most suitable date and were verified repeatedly for 3 years. As a result, it has been revealed that corn and sunflower yield can be determined on a parcel basis with a single satellite image with an average relative error of 0.10.

When estimating yield with a single satellite image, satellite image selection should be made taking into account the fact that different agricultural plants will be planted in the region and the differences in the development speed and duration of these plants. When determining single-dated images, the most appropriate period should be selected by taking into account the development status of the species planted at the same or recently.

References

Adamsen, F. J., Pinter Jr, P. J., Barnes, E. M., LaMorte, R. L., Wall, G. W., Leavitt, S. W., & Kimball, B. A. (1999). Measuring wheat senescence with a digital camera. *Crop science*, *39*(3), 719-724.

Ahl, D. E., Gower, S. T., Mackay, D. S., Burrows, S. N., Norman, J. M., & Diak, G. R. (2004). Heterogeneity of light use efficiency in a northern Wisconsin forest: implications for modeling net primary production with remote sensing. *Remote Sensing of Environment*, *93*(1-2), 168-178.

Algancı, U. (2014). *Uydu Görüntüleri, Meteorolojik Veriler Ve Kamera Fotoğrafları İle Pamuk Ve Mısır Bitkileri İçin Rekolte Tahmin Modeli Tasarımı: Şanlıurfa Örneği* (Doctoral dissertation, Fen Bilimleri Enstitüsü).

Alganci, U., Ozdogan, M., Sertel, E., & Ormeci, C. (2014). Estimating maize and cotton yield in southeastern Turkey with integrated use of satellite images, meteorological data and digital photographs. *Field Crops Research*, *157*, 8-19.

Almalki, R., Khaki, M., Saco, P. M., & Rodriguez, J. F. (2022). Monitoring and mapping vegetation cover changes in arid and semi-arid areas using remote sensing technology: a review. *Remote Sensing*, *14*(20), 5143.

Anderson, E. L. (1988). Tillage and N fertilization effects on maize root growth and root: shoot ratio. *Plant and Soil*, *108*, 245-251.

Asrar, G. Q., Fuchs, M., Kanemasu, E. T., & Hatfield, J. L. (1984). Estimating absorbed photosynthetic radiation and leaf area index from spectral reflectance in wheat 1. *Agronomy journal*, *76*(2), 300-306.

Bandaru, V., West, T. O., Ricciuto, D. M., & Izaurralde, R. C. (2013). Estimating crop net primary production using national inventory data and MODIS-derived parameters. *ISPRS Journal of Photogrammetry and Remote Sensing*, *80*, 61-71.

Baret, F., Guyot, G., & Major, D. J. (1989). Crop biomass evaluation using radiometric measurements. *Photogrammetria*, *43*(5), 241-256.

Baret, F., Hagolle, O., Geiger, B., Bicheron, P., Miras, B., Huc, M., ... & Leroy, M. (2007). LAI, fAPAR and fCover CYCLOPES global products derived from VEGETATION: Part 1: Principles of the algorithm. *Remote sensing of environment*, *110*(3), 275-286.

Barr, J. G., Engel, V., Fuentes, J. D., Fuller, D. O., & Kwon, H. (2013). Modeling light use efficiency in a subtropical mangrove forest equipped with CO 2 eddy covariance. *Biogeosciences*, *10*(3), 2145-2158.

Bastiaanssen, W. G., & Ali, S. (2003). A new crop yield forecasting model based on satellite measurements applied across the Indus Basin, Pakistan. *Agriculture, ecosystems & environment*, *94*(3), 321-340.

Bazgir, S., Kamali, G., & Mortazavi, A. (2007). Wheat yield prediction through agrometeorological indices for Hamedan, Iran.

Bernstein, L. S., Jin, X., Gregor, B., & Adler-Golden, S. M. (2012). Quick atmospheric correction code: algorithm description and recent upgrades. *Optical engineering*, *51*(11), 111719-111719.
Bréda, N. J. (2003). Ground-based measurements of leaf area index: a review of methods, instruments and current controversies. *Journal of experimental botany*, *54*(392), 2403-2417.
Drolet, G. G., Middleton, E. M., Huemmrich, K. F., Hall, F. G., Amiro, B. D., Barr, A. G., ... & Margolis, H. A. (2008). Regional mapping of gross light-use efficiency using MODIS spectral indices. *Remote Sensing of Environment*, *112*(6), 3064-3078.
Dwyer, L. M., Ma, B. L., Evenson, L., & Hamilton, R. I. (1994). Maize physiological traits related to grain yield and harvest moisture in mid-to short-season environments. *Crop Science*, *34*(4), 985-992.
Dye, D. G., & Shibasaki, R. (1995). Intercomparison of global PAR data sets. *Geophysical Research Letters*, *22*(15), 2013-2016.
Dymond, J. R., Stephens, P. R., Newsome, P. F., & Wilde, R. H. (1992). Percentage vegetation cover of a degrading rangeland from SPOT. *International journal of remote sensing*, *13*(11), 1999-2007.
Elmore, A. J., Mustard, J. F., Manning, S. J., & Lobell, D. B. (2000). Quantifying vegetation change in semiarid environments: precision and accuracy of spectral mixture analysis and the normalized difference vegetation index. *Remote sensing of environment*, *73*(1), 87-102.
Elvidge, C. D., & Chen, Z. (1995). Comparison of broad-band and narrow-band red and near-infrared vegetation indices. *Remote sensing of environment*, *54*(1), 38-48.
Ewing, R. P., & Horton, R. (1999). Quantitative color image analysis of agronomic images. *Agronomy Journal*, *91*(1), 148-153.
Faria, F. A., dos Santos, J. A., Torres, R. D. S., Rocha, A., & Falcao, A. X. (2012, July). Automatic fusion of region-based classifiers for coffee crop recognition. In *2012 IEEE International Geoscience and Remote Sensing Symposium* (pp. 2221-2224). IEEE.
Field, C. B., Randerson, J. T., & Malmström, C. M. (1995). Global net primary production: combining ecology and remote sensing. *Remote sensing of Environment*, *51*(1), 74-88.
Gitelson, A. A., Kaufman, Y. J., & Merzlyak, M. N. (1996). Use of a green channel in remote sensing of global vegetation from EOS-MODIS. *Remote sensing of Environment*, *58*(3), 289-298.
Gitelson, A. A., Kaufman, Y. J., Stark, R., & Rundquist, D. (2002). Novel algorithms for remote estimation of vegetation fraction. *Remote sensing of Environment*, *80*(1), 76-87.
Gitelson, A. A., Peng, Y., Masek, J. G., Rundquist, D. C., Verma, S., Suyker, A., ... & Meyers, T. (2012). Remote estimation of crop gross primary production with Landsat data. *Remote Sensing of Environment*, *121*, 404-414.
Godínez-Alvarez, H., Herrick, J. E., Mattocks, M., Toledo, D., & Van Zee, J. (2009). Comparison of three vegetation monitoring methods: Their relative utility for ecological assessment and monitoring. *Ecological indicators*, *9*(5), 1001-1008.
Goetz, S. J., & Prince, S. D. (1999). Modelling terrestrial carbon exchange and storage: evidence and implications of functional convergence in light-use efficiency. In *Advances in ecological research* (Vol. 28, pp. 57-92). Academic Press.
Guo, C., Zhang, L., Zhou, X., Zhu, Y., Cao, W., Qiu, X., ... & Tian, Y. (2018). Integrating remote sensing information with crop model to monitor wheat growth and yield based on simulation zone partitioning. *Precision agriculture*, *19*, 55-78.
Gürbüz, B., Kaya, M. D., & Demirtola, A. (2003). Ayçiçeği tarımı. Hasat Yayıncılık Ltd. Şti. *Ege Basım*.
Hall, F. G., Huemmrich, K. F., Goetz, S. J., Sellers, P. J., & Nickeson, J. E. (1992). Satellite remote sensing of surface energy balance: Success, failures, and unresolved issues in FIFE. *Journal of Geophysical Research: Atmospheres*, *97*(D17), 19061-19089.
Hay, G. J., Dubé, P., Bouchard, A., & Marceau, D. J. (2002). A scale-space primer for exploring and quantifying complex landscapes. *Ecological Modelling*, *153*(1-2), 27-49.
He, M., Kimball, J. S., Maneta, M. P., Maxwell, B. D., Moreno, A., Beguería, S., & Wu, X. (2018). Regional crop gross primary productivity and yield estimation using fused landsat-MODIS data. *Remote Sensing*, *10*(3), 372.
Hemming, J., & Rath, T. (2001). PA—Precision agriculture: Computer-vision-based weed identification under field conditions using controlled lighting. *Journal of agricultural engineering research*, *78*(3), 233-243.
Herrick, J. E., Bestelmeyer, B. T., Archer, S., Tugel, A. J., & Brown, J. R. (2006). An integrated framework for science-based arid land management. *Journal of Arid Environments*, *65*(2), 319-335.
Hoberg, T., & Müller, S. (2011). Multitemporal crop type classification using conditional random fields and RapidEye data. *The International Archives of the Photogrammetry, Remote Sensing and Spatial Information Sciences; XXXVIII-4/W19*, *38*(W19), 115-121.
Holben, B. N. (1986). Characteristics of maximum-value composite images from temporal AVHRR data. *International journal of remote sensing*, *7*(11), 1417-1434.

Houborg, R., Anderson, M. C., Daughtry, C. S. T., Kustas, W. P., & Rodell, M. (2011). Using leaf chlorophyll to parameterize light-use-efficiency within a thermal-based carbon, water and energy exchange model. *Remote Sensing of Environment*, *115*(7), 1694-1705.

Huang, C., Davis, L. S., & Townshend, J. R. G. (2002). An assessment of support vector machines for land cover classification. *International Journal of remote sensing*, *23*(4), 725-749.

Huete, A. R. (1988). A soil-adjusted vegetation index (SAVI). *Remote sensing of environment*, *25*(3), 295-309.

Ines, A. V., & Honda, K. (2005). On quantifying agricultural and water management practices from low spatial resolution RS data using genetic algorithms: A numerical study for mixed-pixel environment. *Advances in Water Resources*, *28*(8), 856-870.

Jensen, J. R. (2005). Digital image processing: a remote sensing perspective. *Upper Saddle River, NJ: sPrentice Hall*.

Jin, X., Li, Z., Feng, H., Ren, Z., & Li, S. (2020). Estimation of maize yield by assimilating biomass and canopy cover derived from hyperspectral data into the AquaCrop model. *Agricultural Water Management*, *227*, 105846.

Jones, H. G., & Vaughan, R. A. (2010). *Remote sensing of vegetation: principles, techniques, and applications*. Oxford University Press, USA.

Jongschaap, R. E. (2007). Sensitivity of a crop growth simulation model to variation in LAI and canopy nitrogen used for run-time calibration. *Ecological Modelling*, *200*(1-2), 89-98.

Karakus, P., & Karabork, H. (2017). Estimating crop cover fraction from digital color images. *The International Archives of the Photogrammetry, Remote Sensing and Spatial Information Sciences*, *42*, 67-68.

Karakus, P., & Karabörk, H. (2020). Crop Cover Fraction Estimation Based On Digital Images from 2014-2016: A Case Study of Kadirli in Osmaniye Province. *Türkiye Uzaktan Algılama Dergisi*, *2*(2), 50-57.

Karthikeyan, L., Chawla, I., & Mishra, A. K. (2020). A review of remote sensing applications in agriculture for food security: Crop growth and yield, irrigation, and crop losses. *Journal of Hydrology*, *586*, 124905.

Kaushalya Madhavi, B. G., Bhujel, A., Kim, N. E., & Kim, H. T. (2022). Measurement of overlapping leaf area of ice plants using digital image processing technique. *Agriculture*, *12*(9), 1321.

Kırtok, Y. (1998). *Mısır: üretimi ve kullanımı*. Kocaoluk Yayınevi.

Kross, A., Seaquist, J. W., & Roulet, N. T. (2016). Light use efficiency of peatlands: Variability and suitability for modeling ecosystem production. *Remote Sensing of Environment*, *183*, 239-249.

Laliberte, A. S., Rango, A., Herrick, J. E., Fredrickson, E. L., & Burkett, L. (2007). An object-based image analysis approach for determining fractional cover of senescent and green vegetation with digital plot photography. *Journal of Arid Environments*, *69*(1), 1-14.

Leite, P. B. C., Feitosa, R. Q., Formaggio, A. R., da Costa, G. A. O. P., Pakzad, K., & Sanches, I. D. A. (2011). Hidden Markov Models for crop recognition in remote sensing image sequences. *Pattern Recognition Letters*, *32*(1), 19-26.

Li, J. F., Wang, K. Q., & Zhang, D. (2002, November). A new equation of saturation in RGB-to-HSI conversion for more rapidity of computing. In *Proceedings. International Conference on Machine Learning and Cybernetics* (Vol. 3, pp. 1493-1497). IEEE.

Li, Y., Chen, D., Walker, C. N., & Angus, J. F. (2010). Estimating the nitrogen status of crops using a digital camera. *Field Crops Research*, *118*(3), 221-227.

Liu, H. Q., & Huete, A. (1995). A feedback based modification of the NDVI to minimize canopy background and atmospheric noise. *IEEE transactions on geoscience and remote sensing*, *33*(2), 457-465.

Liu, J., & Pattey, E. (2010). Retrieval of leaf area index from top-of-canopy digital photography over agricultural crops. *Agricultural and Forest Meteorology*, *150*(11), 1485-1490.

Liu, Y., Mu, X., Wang, H., & Yan, G. (2012). A novel method for extracting green fractional vegetation cover from digital images. *Journal of Vegetation Science*, *23*(3), 406-418.

Lobell, D. B., Asner, G. P., Ortiz-Monasterio, J. I., & Benning, T. L. (2003). Remote sensing of regional crop production in the Yaqui Valley, Mexico: estimates and uncertainties. *Agriculture, Ecosystems & Environment*, *94*(2), 205-220.

Lukina, E. V., Stone, M. L., & Raun, W. R. (1999). Estimating vegetation coverage in wheat using digital images. *Journal of Plant Nutrition*, *22*(2), 341-350.

McCallum, I., Wagner, W., Schmullius, C., Shvidenko, A., Obersteiner, M., Fritz, S., & Nilsson, S. (2009). Satellite-based terrestrial production efficiency modeling. *Carbon balance and management*, *4*, 1-14.

Monteith, J. L. (1972). Solar radiation and productivity in tropical ecosystems. *Journal of applied ecology*, *9*(3), 747-766.

Monteith, J. L. (1977). Climate and the efficiency of crop production in Britain. *Philosophical transactions of the royal society of London. B, Biological Sciences*, *281*(980), 277-294.

Moran, M. S., Maas, S. J., & Pinter Jr, P. J. (1995). Combining remote sensing and modeling for estimating surface evaporation and biomass production. *Remote Sensing Reviews*, *12*(3-4), 335-353.

Myneni, R. B., Hall, F. G., Sellers, P. J., & Marshak, A. L. (1995). The interpretation of spectral vegetation indexes. *IEEE Transactions on Geoscience and remote Sensing*, *33*(2), 481-486.

Myneni, R. B., Keeling, C. D., Tucker, C. J., Asrar, G., & Nemani, R. R. (1997a). Increased plant growth in the northern high latitudes from 1981 to 1991. *Nature*, *386*(6626), 698-702.

Myneni, R. B., Ramakrishna, R., Nemani, R. O. E. N. T. G. E. N., & Running, S. W. (1997b). Estimation of global leaf area index and absorbed PAR using radiative transfer models. *IEEE Transactions on Geoscience and remote sensing*, *35*(6), 1380-1393.

Olofsson, P., Eklundh, L., Lagergren, F., Jönsson, P., & Lindroth, A. (2007). Estimating net primary production for Scandinavian forests using data from Terra/MODIS. *Advances in Space Research*, *39*(1), 125-130.

Onurlubaş, H. E., & Kızılaslan, H. (2007). Türkiye'de bitkisel yağ sanayindeki gelişmeler ve geleceğe yönelik beklentiler. *Tarım Ekonomisi Araştırma Enstitüsü*, *157*, 1-72.

Pan, G., Li, F. M., & Sun, G. J. (2007, July). Digital camera based measurement of crop cover for wheat yield prediction. In *2007 IEEE International Geoscience and Remote Sensing Symposium* (pp. 797-800). IEEE.

Peña-Barragán, J. M., Ngugi, M. K., Plant, R. E., & Six, J. (2011). Object-based crop identification using multiple vegetation indices, textural features and crop phenology. *Remote Sensing of Environment*, *115*(6), 1301-1316.

Peng, Y., Li, Y., Dai, C., Fang, S., Gong, Y., Wu, X., ... & Liu, K. (2019). Remote prediction of yield based on LAI estimation in oilseed rape under different planting methods and nitrogen fertilizer applications. *Agricultural and forest meteorology*, *271*, 116-125.

Poblete-Echeverría, C., Fuentes, S., Ortega-Farias, S., Gonzalez-Talice, J., & Yuri, J. A. (2015). Digital cover photography for estimating leaf area index (LAI) in apple trees using a variable light extinction coefficient. *Sensors*, *15*(2), 2860-2872.

Potter, C. S., Randerson, J. T., Field, C. B., Matson, P. A., Vitousek, P. M., Mooney, H. A., & Klooster, S. A. (1993). Terrestrial ecosystem production: A process model based on global satellite and surface data. *Global biogeochemical cycles*, *7*(4), 811-841.

Prince, S. D., & Goward, S. N. (1995). Global primary production: a remote sensing approach. *Journal of biogeography*, 815-835.

Propastin, P. A., Kappas, M. W., Herrmann, S. M., & Tucker, C. J. (2012). Modified light use efficiency model for assessment of carbon sequestration in grasslands of Kazakhstan: combining ground biomass data and remote-sensing. *International Journal of Remote Sensing*, *33*(5), 1465-1487.

Purevdorj, T. S., Tateishi, R., Ishiyama, T., & Honda, Y. (1998). Relationships between percent vegetation cover and vegetation indices. *International journal of remote sensing*, *19*(18), 3519-3535.

Qin, H., Wang, C., Zhao, K., & Xi, X. (2018). Estimation of the fraction of absorbed photosynthetically active radiation (fPAR) in maize canopies using LiDAR data and hyperspectral imagery. *Plos one*, *13*(5), e0197510.

Raich, J. W., Rastetter, E. B., Melillo, J. M., Kicklighter, D. W., Steudler, P. A., Peterson, B. J., ... & Vorosmarty, C. J. (1991). Potential net primary productivity in South America: application of a global model. *Ecological applications*, *1*(4), 399-429.

Richardson, M. D., Karcher, D. E., & Purcell, L. C. (2001). Quantifying turfgrass cover using digital image analysis. *Crop Science*, *41*(6), 1884-1888.

Rouse, J. W., Haas, R. H., Schell, J. A., & Deering, D. W. (1974). Monitoring vegetation systems in the Great Plains with ERTS. *NASA Spec. Publ*, *351*(1), 309.

Running, S. W., Nemani, R. R., Heinsch, F. A., Zhao, M., Reeves, M., & Hashimoto, H. (2004). A continuous satellite-derived measure of global terrestrial primary production. *Bioscience*, *54*(6), 547-560.

Ryherd S, Woodcock C (1996). Combining spectral and texture data in the segmentation of remotely sensed images. Photogrammetric engineering and remote sensing 62:181-194.

Sala, O. E., & Paruelo, J. M. (1997). Ecosystem services in grasslands. *Nature's services: Societal dependence on natural ecosystems*, 237-251.

Sandhu, H. A. S., Gusain, H. S., Arora, M. K., & Bawa, A. (2018). Mass balance estimation of dokriani glacier in central Indian himalaya using remote sensing data. *Journal of the Indian Society of Remote Sensing*, *46*, 1835-1840.

Sandhu, S. S., Kaur, P., Singh, J., Nigam, R., & Gill, K. K. (2019). Evaluation of greencrop tracker for the estimation of leaf area index in wheat using digital photography. *Proceedings of the National Academy of Sciences, India Section B: Biological Sciences*, *89*, 615-621.

Seaquist, J. W., Olsson, L., & Ardö, J. (2003). A remote sensing-based primary production model for grassland biomes. *Ecological Modelling*, *169*(1), 131-155.

Senseman, G. M., Bagley, C. F., & Tweddale, S. A. (1996). Correlation of rangeland cover measures to satellite-imagery-derived vegetation indices. *Geocarto International*, *11*(3), 29-38.

Sripada, R. P., Heiniger, R. W., White, J. G., & Meijer, A. D. (2006). Aerial color infrared photography for determining early in-season nitrogen requirements in corn. *Agronomy Journal*, *98*(4), 968-977.

Soltani, A., Torabi, B., & Zarei, H. (2005). Modeling crop yield using a modified harvest index-based approach: application in chickpea. *Field crops research*, *91*(2-3), 273-285.

Suarez Baron, M. J., Gomez, A. L., & Diaz, J. E. E. (2022). Supervised learning-based image classification for the detection of late blight in potato crops. *Applied Sciences*, *12*(18), 9371.

Sykes, A. O. (1993). An introduction to regression analysis.

Tang, L., Tian, L., & Steward, B. L. (2000). Color image segmentation with genetic algorithm for in-field weed sensing. *Transactions of the ASAE*, *43*(4), 1019-1027.

Tao, F., Yokozawa, M., Hayashi, Y., & Lin, E. (2003). Changes in agricultural water demands and soil moisture in China over the last half-century and their effects on agricultural production. *Agricultural and Forest Meteorology*, *118*(3-4), 251-261.

Tao, F., Yokozawa, M., Zhang, Z., Xu, Y., & Hayashi, Y. (2005). Remote sensing of crop production in China by production efficiency models: models comparisons, estimates and uncertainties. *Ecological modelling*, *183*(4), 385-396.

Türkoğlu, A. (1971). Gıda maddeleri iktisadi coğrafya 1. *Kitap. İst Matbaası*, *44*.

Viña, A., & Gitelson, A. A. (2005). New developments in the remote estimation of the fraction of absorbed photosynthetically active radiation in crops. *Geophysical research letters*, *32*(17).

Wellington, M. J., Kuhnert, P., Renzullo, L. J., & Lawes, R. (2022). Modelling within-season variation in light use efficiency enhances productivity estimates for cropland. *Remote Sensing*, *14*(6), 1495.

Xiao, Z., Wang, T., Liang, S., & Sun, R. (2016). Estimating the fractional vegetation cover from GLASS leaf area index product. *Remote Sensing*, *8*(4), 337.

Yang, C., Everitt, J. H., & Murden, D. (2011). Evaluating high resolution SPOT 5 satellite imagery for crop identification. *Computers and Electronics in Agriculture*, *75*(2), 347-354.

Yuan, W., Liu, S., Zhou, G., Zhou, G., Tieszen, L. L., Baldocchi, D., ... & Wofsy, S. C. (2007). Deriving a light use efficiency model from eddy covariance flux data for predicting daily gross primary production across biomes. *Agricultural and Forest Meteorology*, *143*(3-4), 189-207.

Yuan, W., Chen, Y., Xia, J., Dong, W., Magliulo, V., Moors, E., ... & Zhang, H. (2016). Estimating crop yield using a satellite-based light use efficiency model. *Ecological Indicators*, *60*, 702-709.

Zhao, Y., Potgieter, A. B., Zhang, M., Wu, B., & Hammer, G. L. (2020). Predicting wheat yield at the field scale by combining high-resolution Sentinel-2 satellite imagery and crop modelling. *Remote Sensing*, *12*(6), 1024.

Zhou, Q., Robson, M., & Pilesjo, P. (1998). On the ground estimation of vegetation cover in Australian rangelands. *International Journal of Remote Sensing*, *19*(9), 1815-1820.

Zhou, Q., & Robson, M. (2001). Automated rangeland vegetation cover and density estimation using ground digital images and a spectral-contextual classifier. *International Journal of Remote Sensing*, *22*(17), 3457-3470.

Url-1 Kadirlibelediyesi, 2016, kadirli, http://www.kadirli.bel.tr/kadirli.html: 12.11.2016

Url-2 ToprakveAraziSınıflamasıStandartlarıTeknikTalimatı, 2005. 05.07.2014

Url-3 (www-cger.nies.go.jp/lugec/Proceedings/32Tsunekawa.pdf) 22.04.2015